Bi-directional conversion between microwave and optical frequencies in a piezoelectric optomechanical device

Amit Vainsencher,[1] K. J. Satzinger,[2] G. A. Peairs,[2] and A. N. Cleland[2]
[1]*Department of Physics, University of California, Santa Barbara, California 93106, USA*
[2]*Institute for Molecular Engineering, University of Chicago, Chicago, Illinois 60637, USA*

We describe the principles of design, fabrication, and operation of a piezoelectric optomechanical crystal with which we demonstrate bi-directional conversion of energy between microwave and optical frequencies. The optomechanical crystal has an optical mode at 1523 nm co-located with a mechanical breathing mode at 3.8 GHz, with a measured optomechanical coupling strength $g_{om}/2\pi$ of 115 kHz. The breathing mode is driven and detected by curved interdigitated transducers that couple to a Lamb mode in suspended membranes on either end of the optomechanical crystal, allowing the external piezoelectric modulation of the optical signal as well as the converse, the detection of microwave electrical signals generated by a modulated optical signal. We compare measurements to theory where appropriate. *Published by AIP Publishing.* [http://dx.doi.org/10.1063/1.4955408]

Engineered quantum systems have undergone a revolution in both the performance of individual quantum bits as well as the number of qubits that can be coupled to one another.[1–3] However, much of the progress in these engineered systems has been with microwave frequency qubits, especially in superconducting implementations. This makes long-distance communication of any quantum information generated in these systems very challenging, due to the presence of the large microwave background in a non-cryogenic environment. As a result, there are a number of distinct efforts to coherently couple microwave quantum signals to optical ones,[4–10] as this could combine the high fidelity quantum control achievable with engineered microwave qubits with the long distance communication possible with optical photons.

Here, we describe an important step forward in one such approach, where we use a piezoelectric optomechanical device with integrated electromechanical transduction to demonstrate bi-directional coherent transduction between microwave frequencies and an optical signal in a common telecommunications band. The device includes electromechanical transducers that are mode-matched to itinerant Lamb wave phonons,[11,12] which are in turn coupled to a mechanically suspended optomechanical crystal (OMC)[13] supporting a localized mechanical breathing mode. The breathing mode is co-located with a localized optical mode, where strong optomechanical coupling between these two modes yields the desired frequency transduction. The microwave mechanical frequency of these devices is designed to match that of superconducting qubits, yielding a straightforward integration with these quantum systems. In previous work with microwave frequency mechanical modes in the GHz band, experiments have shown electrical to optical conversion, but not the reverse.[5,6] Bi-directional operation has been challenging due to the difficulty in simultaneously achieving strong electromechanical coupling and good mode matching to the appropriate microwave frequency mechanical mode, especially as the requisite structures span dimensions corresponding to hundreds of mechanical wavelengths.[14]

The material system we chose for exploring this approach is aluminum nitride (AlN), a material that allows growth of oriented polycrystalline thin films when reactively sputtered on a thick layer of oxidized silicon.[5,6] AlN grown in this fashion has a significant piezoelectric response, which allows for strong electromechanical coupling via metallic electrodes.[15] The relevant piezoelectric coefficients are[16] $\epsilon_{33} \approx 1.46$ C/m^2 and $\epsilon_{31} \approx -0.60$ C/m^2. The excellent optical properties of properly prepared films of AlN also allow the fabrication of high quality photonic components, including low-loss optical resonators, waveguides, and optomechanical crystals. Structures made from this material may be mechanically suspended by selectively removing the underlying oxide, yielding free-standing structures with low mechanical and optical loss.

Using this platform, we have designed and fabricated devices in which an optimized OMC[17] is mechanically coupled to an interdigitated Lamb wave transducer (IDT). The overall device design and key elements are shown in Fig. 1, along with numerical simulations of the relevant optical and mechanical modes. The electromechanical transducers are designed to efficiently couple to phonons emitted from the ends of the OMC with a radial radiation pattern, as predicted by finite element simulations. The pitch of the electrodes selects a zero-order symmetric Lamb wave of the appropriate wavelength, closely matched to an in-plane resonance of the underlying two-dimensional plate structure, and resonant with the OMC breathing mode.

The device fabrication involved two steps of photolithography followed by one step of electron beam lithography, followed by three more steps of photolithography. Fabrication started on a 100 mm Si wafer on which we grew 3.17 μm of thermal SiO$_2$ followed by oriented sputtering of 330 nm of c-axis oriented AlN, followed by 150 nm of aluminum. In the first process step, the Al wiring was defined by photolithography followed by a chlorine plasma etch. A second photolithography step then defined 10 nm chrome-150 nm gold alignment marks. An etch mask in hydrogen silsesquioxane resist was then defined by electron beam lithography, for etch patterning of the nanostructures (the optomechanical and
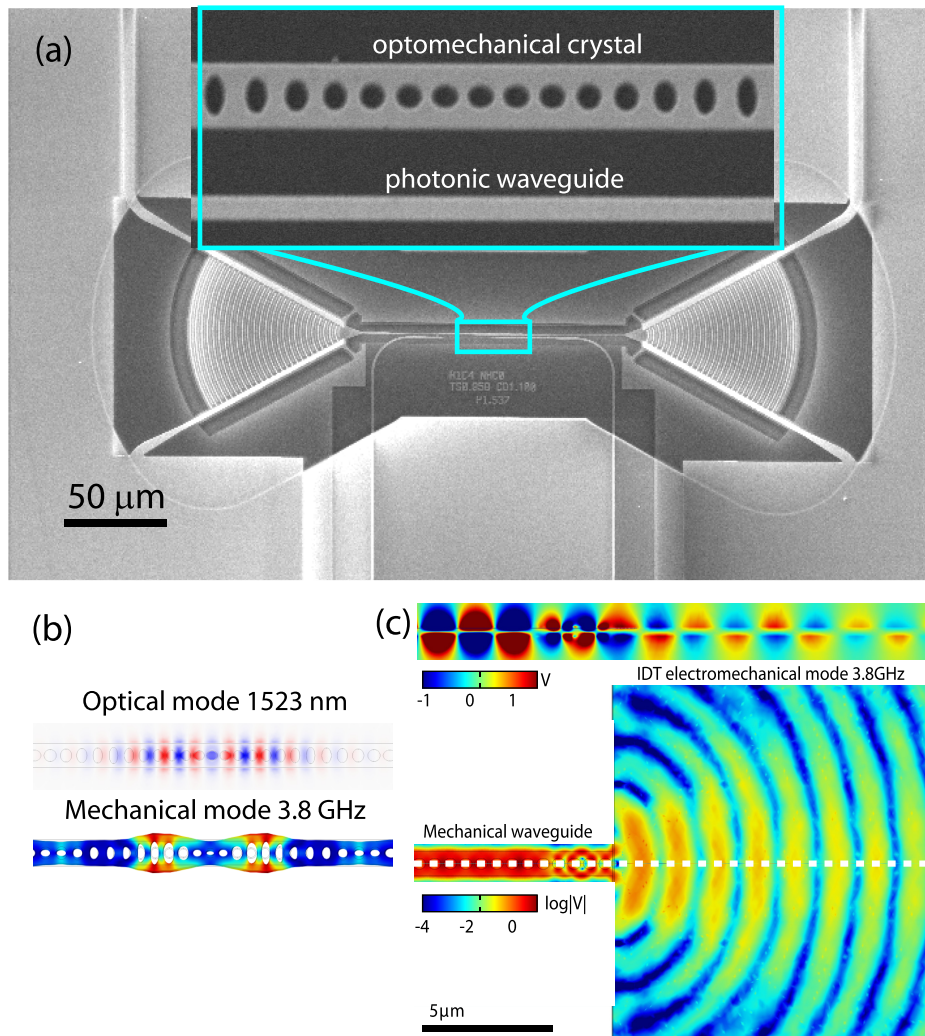
FIG. 1. (a) Overview of device geometry, comprising a pair of radially symmetric Lamb wave IDTs coupled to an optomechanical crystal. The OMC is patterned from a 330 nm thick layer of free standing AlN, and the IDTs are patterned from a top layer of 150 nm thick aluminum. (b) Finite element simulation of the relevant optical mode in the OMC (upper), along with a finite element simulation of the relevant mechanical mode (lower). (c) Upper: Side cutaway of voltage as itinerant mechanical waves transition from the OMC to a half-infinite plate of matching thickness. The induced voltage is indicative of symmetric Lamb waves. Lower: Top view of the structure, with color indicating log magnitude of voltage. These simulations are a conceptual guide, but they do not account for the wedge transition region or the tethers in the actual device. Including these features produces qualitatively similar results but with additional distortion of the mode shape due to changes in the plate's mechanical resonance.

photonic structures, as well as the interdigitated (IDT) electrodes). Following additional masking of some of the area with a third photolithography step, the IDT pattern was etched into the Al and AlN; after removing the photoresist, two more masking layers of photoresist were defined with intervening etches of the optical and optomechanical structures. In the final step, the underlying oxide was removed using a vapor hydrofluoric etch tool, in such a way that the exposed Al and AlN were not damaged.

The electrodes for each IDT, remote from the OMC, are alternately wired to signal and ground, with the signal connected to the center trace of a 50 Ω microwave coplanar waveguide, leading to a microwave launcher; each launcher is contacted by a microwave probe. The localized optical mode in the OMC has a 1523 nm design wavelength and a 3.8 GHz mechanical breathing mode frequency. The OMC was optically probed through an evanescently coupled integrated photonic waveguide, whose ends terminate in radial grating couplers for coupling to a pair of optical fibers.

Figure 2 shows characterization measurements of the device at room temperature. Sweeping the laser frequency ω_l reveals the relevant OMC resonance at ω_o as a dip in the measured optical transmission when $\omega_l = \omega_o$ (inset). A fit to this feature yields a coupled loss rate of $\kappa/2\pi = 15.2$ GHz, with an intrinsic loss rate $\kappa_i/2\pi = 4.7$ GHz. By locking the laser to the side of the optical resonance (green center arrow

in inset), we can detect sidebands induced on the transmitted signal by the mechanical breathing mode's thermal motion, shown in Fig. 2(a), with the peak at the design frequency of 3.78 GHz. The width of the peak corresponds to a mechanical loss rate of $\gamma/2\pi = 5.0$ MHz, and we estimate the intrinsic and extrinsic components of the loss to be $\gamma_i/2\pi = 3.5$ MHz and $\gamma_e/2\pi = 1.5$ MHz. The breathing mode noise peak can be used to extract a coupling rate of $g_{om}/2\pi = 115 \pm 15$ kHz between the localized optical and breathing modes in the OMC.[18]

The IDT electromechanical transducers were characterized by measuring the amplitude of the microwave frequency reflection (S_{11}) with a vector network analyzer (Fig. 2(a), blue). These displayed the expected pronounced dip in reflection at the 3.78 GHz design frequency of the IDTs. Additionally, we measured the microwave transmitted amplitude (S_{ee}) between the two IDTs at either end of the OMC, showing the expected strong coupling at the design frequency of the IDTs (not shown).

We can measure electrical to optical transduction, in which an electrical signal generates a modulation of a transmitted optical signal. This is done by locking the laser to the side of the optical resonance (green center arrow in inset to Fig. 2(a)) and driving either IDT with a microwave frequency electrical tone, while measuring the sidebands generated on the laser signal by using a fast photodetector. The
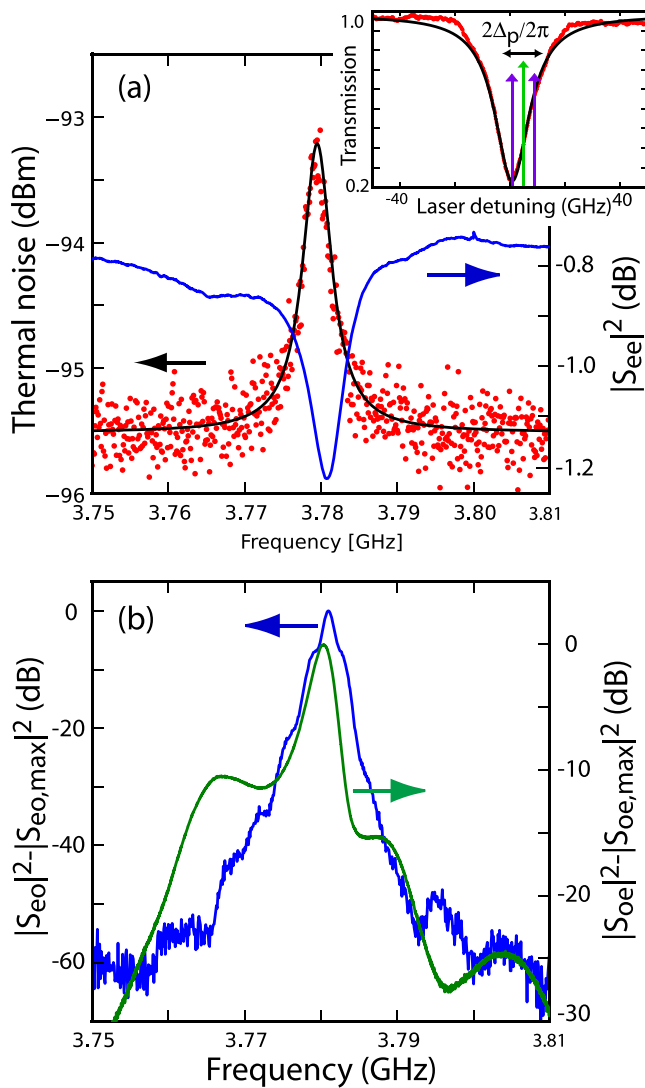
FIG. 2. (a) Inset: Optical resonance of the OMC, shown in red. A Lorentzian fit is superposed in black, with a fit coupled loss rate $\kappa/2\pi = 15.2$ GHz and internal loss rate of $\kappa_i/2\pi = 4.7$ GHz. When reading out the mechanical motion using an optical signal, the laser is tuned to the position of the green center arrow. The green and purple arrows together represent the laser with phase modulated sidebands spaced Δ_p apart, with optical driving of the mechanical mode occurring when $\Delta_p \approx \omega_m$. Main panel: Optical readout of the OMC's mechanical breathing mode's thermal noise at room temperature, shown in red. A Lorentzian fit to the breathing mode is shown in black, with fit mechanical loss rate $\gamma/2\pi = 5.0$ MHz; the amplitude yields $g_{om}/2\pi = 115 \pm 15$ kHz. We also show the measured S_{11} reflection from the right IDT, in blue, showing good frequency matching to the OMC breathing mode. (b) Electrical driving with optical detection is shown in green (S_{oe}). Optical driving of the OMC with electrical detection of the resulting mechanical motion is shown in blue (S_{eo}). Both measurements were completed using the right IDT, although similar results are found using the left IDT.

result of this measurement is shown in Fig. 2(b), showing strong electrical-to-optical transduction (S_{oe}) at the mechanical design frequency of 3.78 GHz.

We can also demonstrate the reverse operation, in which an externally modulated optical signal generates a microwave electrical signal. The optical signal for this measurement consists of a laser tone on which we have imposed sidebands with adjustable amplitudes and sideband frequencies (arrows inset to Fig. 2(a)) using an electro-optic modulator. The beating of the laser tone and the sidebands within the OMC generates an optomechanical force at the sideband

frequency; when this modulation frequency is tuned to the OMC breathing mode frequency, this directly drives the breathing mode amplitude. Phonons are radiated from the leaky OMC and couple to the Lamb wave mode in the two-dimensional supports and are then detected as electrical signals emanating from the IDTs. This measurement (S_{eo}) is shown in blue in Fig. 2(b), where the strongest electrical signal is detected when the laser sidebands are set to the breathing mode frequency of 3.78 GHz.

From these measurements, the internal scattering matrix amplitudes[19] in quanta units can be estimated as $S_{oe,\text{int}} = (0.4 \pm 0.2) \times 10^{-2}$ and $S_{eo,\text{int}} = (1.3 \pm 0.6) \times 10^{-2}$, where $|S_{eo}|^2$ microwave photons are produced for one sideband optical photon, and similarly for S_{oe}. These efficiencies are obtained with intracavity photon populations (at the laser frequency) of $n_{\text{opt}} = 9400$ and 4900 for S_{oe} and S_{eo}, respectively, and are the upper limits of the device efficiency in our measurement setup. While these limits are set by the maximum output power of the laser, the power is also limited by thermal instability in the OMC.

If we include the effects of the IDT impedance mismatch to the external measurement apparatus, and of the optical resonator being sideband-unresolved, we estimate the external efficiencies[20] as $S_{oe,\text{ext}} = (1.4 \pm 0.6) \times 10^{-4}$ and $S_{eo,\text{ext}} = (3.0 \pm 0.9) \times 10^{-4}$.

We note that the conversion efficiencies in both directions do not appear to be equal, even if we extrapolate values for identical n_{opt} (whose value in part determines S). This may be due to nonlinearity in the system on the mechanical driving side resulting in additional loss, as the IDT drive powers used may induce nonlinear mechanical mode conversion in the IDT plate or OMC waveguide. Further study is needed to understand the origin of this asymmetry between S_{oe} and S_{eo}.

We explored the optical driving, electrical readout (S_{eo}) behavior further by varying the laser sideband modulation frequency, central laser frequency, laser power, and sideband power. Some of these measurements are shown in Fig. 3. The intensity plots are in general agreement with theory, some also plotted in Fig. 3. The theoretical predictions are generated by assuming that the beating between the optical carrier and its sidebands results in an optical force driving the mechanical resonator, while ignoring back-action effects. Additionally, we demonstrate phase control of the mechanical resonator, achieved by varying the relative phase of the optical sidebands with respect to a clock signal. The change in the resulting driven mechanical phase is mapped onto a change in the detected electromechanical signal phase, shown in Fig. 3(b).

The successful bilateral operation of this mode-matched electro-optomechanical device holds promise for use as a quantum transducer. However, to demonstrate quantum operation, further improvements must be made. Issues such as understanding the asymmetry in the coupling in either direction, impedance matching the IDTs to readout amplifiers, and improving the optical coupling performance by using other types of fiber-chip coupling,[21] are technical ones that can be solved with established techniques. A more significant challenge is to further increase the optomechanical g_{om}, which may require implementing this type of design in
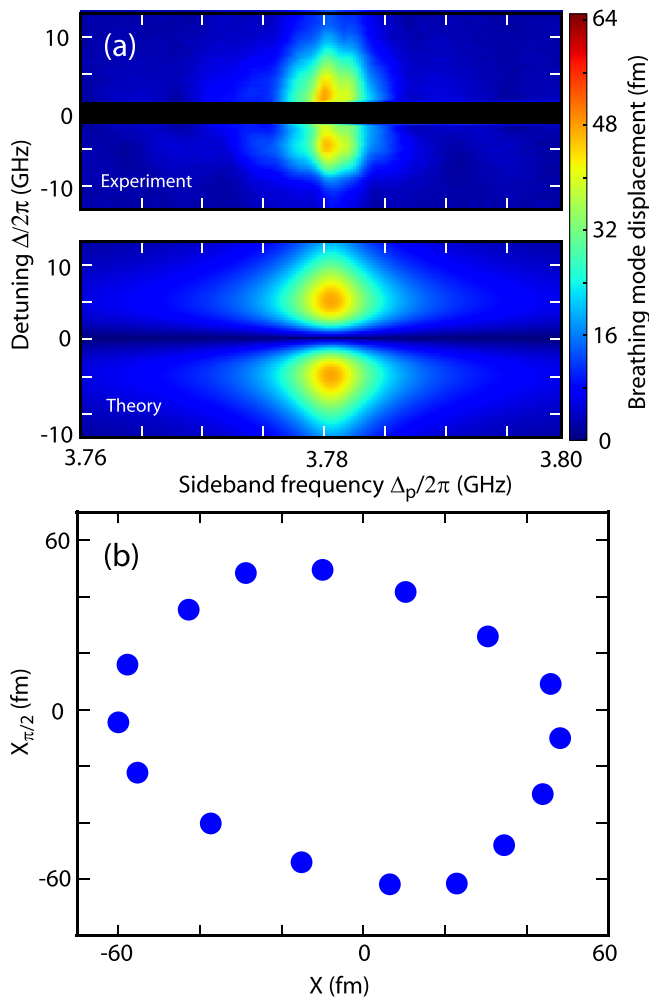
FIG. 3. (a) Intensity plot showing the optically driven, electrically detected motion of the OMC breathing mode, where we varied the laser detuning with respect to the OMC cavity ($\Delta = \omega_o - \omega_l$, vertical axis) and the sideband frequency ($\Delta_p/2\pi$, horizontal axis), while measuring the strength of the electrically detected motion (color scale). Upper plot is measured data while lower plot is theory. Measurement was with fixed carrier and sideband powers $P_0 = 55.2\,\mu W$, $P_{\pm} = 8.6\,\mu W$. (b) Homodyne measurement showing the relation between the detected electromechanical phase as a function of the phase of the sidebands relative to a clock signal, taken with $P_0 = 39\,\mu W$, $P_{\pm} = 16\,\mu W$ and $\Delta = \Delta_p = \omega_m$.

a material with a larger photoelastic response, for example, in silicon[17] or gallium arsenide.[22]

[1]J. Kelly, R. Barends, A. G. Fowler, A. Megrant, E. Jeffrey, T. C. White, D. Sank, J. Y. Mutus, B. Campbell, Y. Chen, Z. Chen, B. Chiaro, A. Dunsworth, I.-C. Hoi, C. Neill, P. J. J. O'Malley, C. Quintana, P. Roushan, A. Vainsencher, J. Wenner, A. N. Cleland, and J. M. Martinis, Nature **519**, 66 (2015).
[2]H. Paik, D. Schuster, L. S. Bishop, G. Kirchmair, G. Catelani, A. Sears, B. Johnson, M. Reagor, L. Frunzio, L. Glazman *et al.*, Phys. Rev. Lett. **107**, 240501 (2011).
[3]K. Eng, T. D. Ladd, A. Smith, M. G. Borselli, A. A. Kiselev, B. H. Fong, K. S. Holabird, T. M. Hazard, B. Huang, P. W. Deelman *et al.*, Sci. Adv. **1**, e1500214 (2015).
[4]C. Regal and K. Lehnert, J. Phys.: Conf. Ser. **264**, 012025 (2011).
[5]J. Bochmann, A. Vainsencher, D. D. Awschalom, and A. N. Cleland, Nat. Phys. **9**, 712 (2013).
[6]C. Xiong, L. Fan, X. Sun, and H. X. Tang, Appl. Phys. Lett. **102**, 021110 (2013).
[7]R. Andrews, R. Peterson, T. Purdy, K. Cicak, R. Simmonds, C. Regal, and K. Lehnert, Nat. Phys. **10**, 321 (2014).
[8]A. Pitanti, J. M. Fink, A. H. Safavi-Naeini, J. T. Hill, C. U. Lei, A. Tredicucci, and O. Painter, Opt. Express **23**, 3196 (2015).
[9]Y. Tabuchi, S. Ishino, A. Noguchi, T. Ishikawa, R. Yamazaki, K. Usami, and Y. Nakamura, Science **349**, 405 (2015).
[10]Y.-D. Wang and A. A. Clerk, Phys. Rev. Lett. **110**, 253601 (2013).
[11]T. Laurent, F. O. Bastien, J.-C. Pommier, A. Cachard, D. Remiens, and E. Cattan, Sens. Actuators, A **87**, 26 (2000).
[12]S. A. Tadesse, H. Li, Q. Liu, and M. Li, Appl. Phys. Lett. **107**, 201113 (2015).
[13]M. Eichenfield, J. Chan, R. M. Camacho, K. J. Vahala, and O. Painter, Nature **462**, 78 (2009).
[14]Bi-directional conversion has been shown in SiN membrane experiments, with a mechanical mode near 1 MHz, with the entire transducer spanning roughly one mechanical wavelength in size.[7]
[15]A. D. O'Connell, M. Hofheinz, M. Ansmann, R. C. Bialczak, M. Lenander, E. Lucero, M. Neeley, D. Sank, H. Wang, M. Weides *et al.*, Nature **464**, 697 (2010).
[16]O. Ambacher, J. Phys. D **31**, 2653 (1998).
[17]J. Chan, A. H. Safavi-Naeini, J. T. Hill, S. Meenehan, and O. Painter, Appl. Phys. Lett. **101**, 081115 (2012).
[18]M. Gorodetsky, A. Schliesser, G. Anetsberger, S. Deleglise, and T. J. Kippenberg, Opt. Express **18**, 23236 (2010).
[19]By internal amplitude, we mean this number has divided out of it the effects of being sideband unresolved, the microwave impedance mismatch between the IDT and 50 Ω microwave environment, and the losses in the grating coupler.
[20]In this case, we consider the input optical signal to be the sum of all sideband power leading to appreciable population within the optical resonator. We also include grating coupler losses.
[21]J. D. Cohen, S. M. Meenehan, and O. Painter, Opt. Express **21**, 11227 (2013).
[22]K. C. Balram, M. Davanço, J. Y. Lim, J. D. Song, and K. Srinivasan, Optica **1**, 414 (2014).